Proceedings of the 9th International Conference on Energy Sustainability
PowerEnergy2015
June 28-July 2, 2015, San Diego, California, USA

PowerEnergy2015-49199

MODELING OF A SOLAR RECEIVER FOR SUPERHEATING SULFURIC ACID

Justin L. Lapp
German Aerospace Center
Cologne, Germany

Alejandro Guerra-Niehoff
German Aerospace Center
Cologne, Germany

Hans-Peter Streber
German Aerospace Center
Cologne, Germany

Dennis Thomey
German Aerospace Center
Cologne, Germany

Martin Roeb
German Aerospace Center
Cologne, Germany

Christian Sattler
German Aerospace Center
Cologne, Germany

ABSTRACT

A volumetric solar receiver for superheating evaporated sulfuric acid is developed as part of a 100kW pilot plant for the Hybrid Sulfur Cycle. The receiver, which uses silicon carbide foam as a heat transfer medium, heats evaporated sulfuric acid using concentrated solar energy to temperatures up to 1000 °C, which are required for the downstream catalytic reaction to split sulfur trioxide into oxygen and sulfur dioxide. Multiple approaches to modeling and analysis of the receiver are performed to design the prototype. Focused numerical modeling and thermodynamic analysis are applied to answer individual design and performance questions. Numerical simulations focused on fluid flow are used to determine the best arrangement of inlets, while thermodynamic analysis is used to evaluate the optimal dimensions and operating parameters. Finally a numerical fluid mechanics and heat transfer model is used to predict the temperature field within the receiver. Important lessons from the modeling efforts are given and their impacts on the design of a prototype are discussed.

INTRODUCTION

The Hybrid Sulfur Cycle (HyS), depicted in Figure 1 is a promising means for storage of sunlight in a chemical fuel, specifically hydrogen [1]. A highly endothermic thermal decomposition of sulfuric acid proceeds at 800–1200 °C, and energy for the reaction can be provided by solar radiation. The decomposition is actually divided into two steps that occur at different temperatures, an evaporation step, and a splitting of sulfur trioxide.

1 (400 °C) $$H_2SO_{4(l)} \rightarrow SO_{3(g)} + H_2O_{(g)} \quad (1)$$

2 (800–1200 °C) $$SO_{3(g)} \rightarrow SO_{2(g)} + \frac{1}{2} O_{2(g)} \quad (2)$$

Typically catalysts are used in step 2 to push the reaction closer to equilibrium. Sulfur dioxide is collected and electrolyzed with water to produce sulfuric acid that is recycled to the first step, and hydrogen, which is collected as a fuel. Though electrical input is required, the voltage requirement of only 0.17 V is much lower than the 1.23 V needed for conventional water electrolysis [1], leading to high process efficiencies from thermal source to fuel [2].

A key step in this cycle is the transfer of solar heat to the sulfuric acid, which occurs at very high temperatures, making it technically challenging. Some concepts for heating sulfuric acid for decomposition relied on inert heat carriers [3,4], or solar powered indirect heating through tubes [5,6]. A complete review of concepts and experiments is given in [7]. To take direct advantage of the high heat fluxes and heat quality of solar radiation, it is desired to transfer heat as directly as possible to the sulfuric acid. This can be accomplished by a directly irradiated porous volumetric absorber as a flow medium for the sulfuric acid. This approach was taken by recent laboratory scale experiments [8].

The current research is part of a project to demonstrate solar heat transfer to sulfuric acid for chemical decomposition using a directly irradiated volumetric absorber at the pilot plant scale. The receiver-absorber itself is part of a larger plant. In order to decouple the sub-processes within the decomposition step, the decomposition plant is divided into three primary

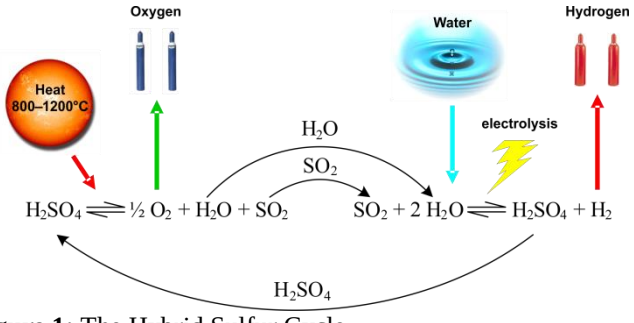

Figure 1: The Hybrid Sulfur Cycle.

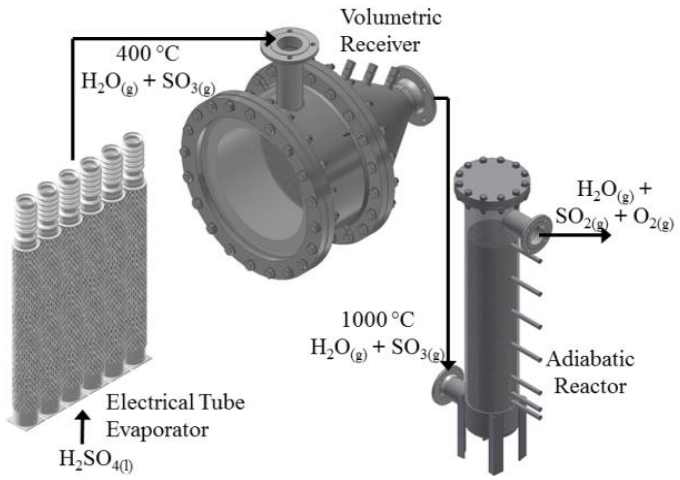

Figure 2: Pilot plant arrangement for decomposition step of sulfuric acid cycle.

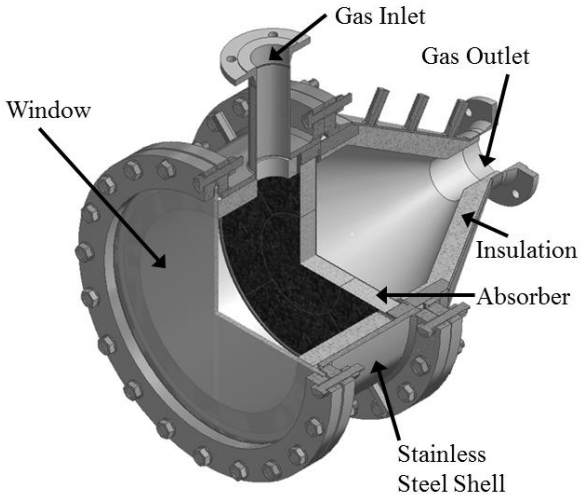

Figure 3: Receiver preliminary design rendering.

devices, as shown in Figure 2. An evaporator, which, for the current pilot experiment will be electrically powered, but for commercial application would likely be powered by medium-concentration solar energy, provides steam and sulfur trioxide from liquid sulfuric acid. The input to the evaporator will be a mixture of sulfuric acid and water, always considered for the present analysis to be 50% each by weight. A volumetric receiver, the subject of current work, heats the gas to about 1000 °C, but without catalysts present, reaction extents will be minor. This device is primarily focused on sensible heating of the gas. A well-insulated, adiabatic reactor will contain catalyst coated particles where the decomposition of sulfur dioxide will occur.

The volumetric receiver itself, with the preliminary design shown in Figure 3, consists of silicon carbide foam absorber, constructed in interlocking sections, a window, a stainless steel shell, and insulation, both inside and outside (not shown) of the shell. The absorber is heated by solar radiation which passes through the window. Evaporated sulfuric acid enters the absorber from the same side as the radiation, and is heated by convective heat transfer as it flows through the foam. This concept has been developed to make the most direct heat transfer possible from sunlight to gas, but also for simplicity and scalability.

The modeling efforts described in this work are focused primarily on selection of suitable and flexible design geometry and operating envelopes, rather than detailed performance validation, system identification, and optimization. Future work will cover these topics. Although the receiver is specific to the Hybrid Sulfur chemical cycle, decoupling the reactor component leads to a device that is almost identical in implementation to air heating or other types of volumetric receivers. A review of solar volumetric receivers, including applications and efforts on modeling of volumetric absorbers, is given in [9].

An analytical model for volumetric solar flow receivers with heat transfer fluids containing nanoparticles was given in [10], with the ability to give performance predictions based on a group of dimensionless numbers, in order to guide design of experimental systems. Lumped system analysis was shown to be a useful tool for evaluation of volumetric air receivers on solar tower systems in [11].

Numerical analysis methods for high temperature porous media are generally applicable to volumetric receivers, the key considerations being (1) the specific transfer of solar spectrum radiation in addition to emitted radiation at longer wavelengths, especially in windowed systems, and (2) the likelihood of local thermal non-equilibrium between the gas and solid within the absorber. Modeling of porous media in solar applications commonly uses volume-averaged techniques, though only a few studies have included coupling of the two factors above.

Early numerical heat transfer analysis of volumetric solar absorbers dates back to analysis of the IEA/SSPS receiver for air heating [12] and the CAESAR project for methane reforming [13], where model predictions were compared with experimental results. A more recent study by Wu et al. included radiative heat transfer coupled to local thermal non-equilibrium (LTNE) energy conservation in a volumetric absorber [14], demonstrating the non-equilibrium effects and model utility with sensitivity studies to various absorber parameters. Villafán-Vidales et al. also considered coupled direct solar radiation and LTNE in a 1 kW absorber and used modeling results to define suitable operating conditions for the receiver reactor [15]. LTNE is considered for a pressurized air receiver system by Hischier et al., and a model is used to examine performance as a function of geometrical and operational parameters [16]. He et al. used LTNE and radiation based models to design pressurized volumetric receivers with a focus on the impacts of uniformity of the solar flux [17]. Other modeling studies of volumetric receivers have been able to account for effects of particulate media [18] and flow stability related to local overheating of absorber material [19].

Foundations of the current analysis have also been completed as part of the predecessor European Union project

HycycleS [20]. Previous work included modeling direct radiation and LTNE in a receiver-reactor [21] and coupling of continuum models with pore-scale property determination [22]. As well, thermodynamic analysis was validated against test results and used to provide suggestions for scaled-up designs [23]. The following analysis focuses on design and feasibility validation of an experimental prototype, using models tailored to answering design questions with minimum complexity.

NOMENCLATURE

A	area, m^2
$\bar{a}$	volume specific surface area, m^{-1}
c_p	specific heat at constant pressure, J kg^{-1} K^{-1}
C,**D**	momentum source term matrices
D	diameter, m
E_b	blackbody emissive power, W m^{-2}
F_{a-b}	view factor from surface *a* to surface *b*
F_{DF}	Dupuit-Forchheimer coefficient
h	convective heat transfer coefficient, W m^{-2} K^{-1}
H_0	external irradiation, W m^{-2}
k	thermal conductivity, W m^{-1} K^{-1}
L	length, m
m	mass, kg
$\dot{m}''$	mass flux, kg s^{-1} m^{-2}
p	pressure, pa
q''	heat flux, W m^{-2}
q'''	volumetric heat source, W m^{-3}
q	heat transfer rate, W
r	radius, m
S	source
T	temperature, K
v	velocity, m s^{-1}
V	volume, m^3
z	axial position, m

Greek

δ_{CSP}	fraction of radiation to absorber
ε	emissivity
ρ	density, kg m^{-3}
ρ	reflectivity
σ	Stefan–Boltzman constant, 5.6704×10^{-8} W $m^{-2}K^{-4}$
τ	transmittance
$\bar{\tau}$	stress tensor
ϕ	volumetric porosity

Subscripts

0	ambient or inlet
abs	absorber or absorbed
conv	convection
CSP	concentrated solar power
emit	emitted radiation
f,s	fluid and solid phase of two phase media
rad	radiation
trans	transmitted
wall	interior wall of receiver body

NUMERICAL FLUID FLOW MODELING

A key initial design decision for the receiver is the placement and design of gas inlets. In order to investigate this design decision, a focused simulation campaign was undertaken. The goal of these simulations is to select a design that minimized complexity while providing a uniform flow field across the absorber area, over a range of flow rates. In the ideal case, this allows an optimized solar field to supply uniform radiation for uniform heating of the gas. In the non-ideal case of non-uniform radiation, it is desired to manage flow distributions as desired by adjusting flow characteristics of the absorber system, without limitations of uncontrollable non-uniformity due to flow inlet design.

A fluid mechanics simulation was developed using ANSYS Fluent to solve standard conservation equations for mass and momentum. Heat transfer was not considered; the system was

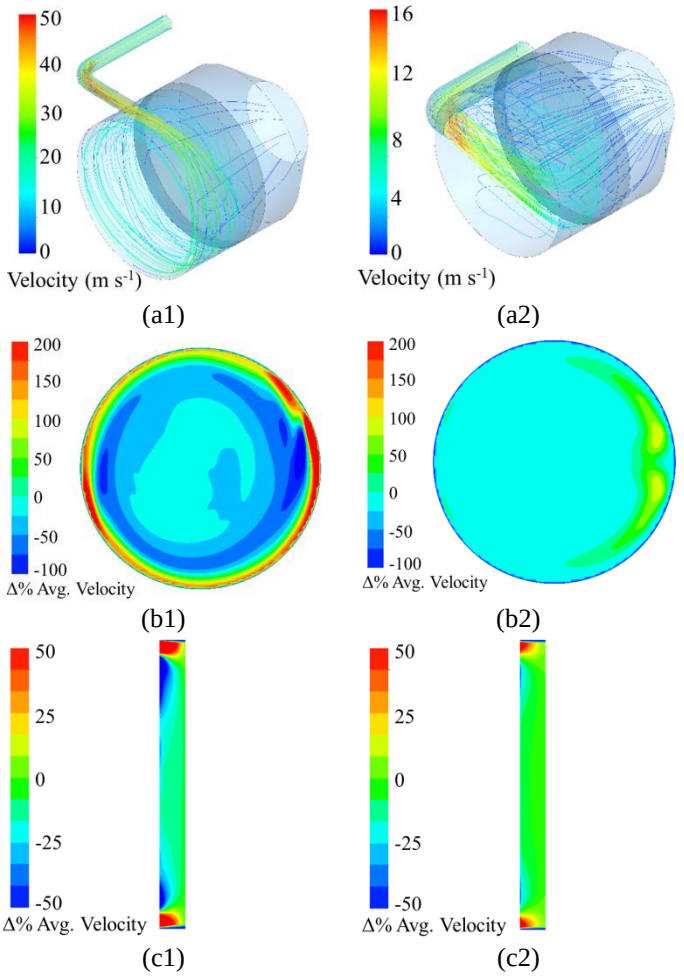

Figure 4: Sample results from isothermal fluid flow modeling of the receiver, showing flow results of (a) velocity streamlines, (b) relative (to average) axial fluid velocity entering absorber, and (c) relative axial velocity on a centerline slice through the absorber. Cases shown are for (1) single tangential gas inlet of 40 mm diameter, and (2) single radial gas inlet of 80 mm diameter. Results from [24].

modeled as isothermal with gas properties taken at 1400 °C for a 50-50 weight mixture of sulfuric acid and water. Additional details are reported in [24].

Simulations considered gas inlets of various diameters, with number of inlets between one and four, and with inlets perpendicular or tangential to the reactor shell. The geometry was based on a preliminary design with a 0.5 m diameter absorber and window. A pressure drop was included at the back surface of the absorber to simulate an orifice plate option in the prototype.

Figure 4 shows a sample of the results from this simulation study. In case (1), a tangential inlet with small diameter leads to high flow through the absorber at the receiver walls, with significant areas of reduced velocity between the walls and the absorber center. In case (2), a single inlet with larger diameter is oriented radially, and leads to greater uniformity of the flow, with an area of slightly above average flow near the wall opposite of the inlet.

Additional simulations explored the option of including an orifice plate at the back edge of the absorber, by simulating with and without the induced pressure drop at this location. It was found that the orifice plate allows for flow uniformity over an increased range of inlet flow conditions for all inlet designs. Based on these results, the receiver design will include this component. The results in Figure 4 are for simulations including this pressure drop layer.

Larger diameter inlets up to a value of 80 mm were found to improve uniformity significantly, while greater values provide little benefit. Radial orientation of the inlets performed better than tangential orientation in all cases. It was found that additional inlets led to improved uniformity, but the improvements were not found to outweigh the added construction complexity. When varied, the axial position of the inlet had little effect. The selected inlet design, based on findings of this simulation work, is a single inlet of 80 mm diameter, oriented radially at the midpoint between absorber and window. Results for this design are shown in Fig. 4, Case 2.

THERMODYNAMIC MODELING

Many factors relating to the performance of the receiver can be studied with a lumped thermodynamic analysis. To study the interaction of radiative heat transfer, component temperature, and gas flow rate, a thermodynamic model of the receiver system was developed as a tool for rapid parametric investigation of several variables. The model couples radiative heat transfer to the window, absorber, and receiver walls to conduction through the reactor walls and convective heat transfer to the gas. It has been used primarily to set receiver geometry and define an operating window of solar flux and gas flow rate values.

Methodology

The thermodynamic model considers first heat transfer from the absorber to the gas, in a one-dimensional sense along the thickness of the absorber. The temperatures along the axial direction in the solid phase of the absorber are characterized by

$$0 = h_{\mathrm{sf}}\,\bar{a}\,(T_{\mathrm{f}} - T_{\mathrm{s}}) + k_{\mathrm{s}}(1-\phi)\frac{\partial^2 T_{\mathrm{s}}}{\partial z^2} \tag{3}$$

where the interfacial heat transfer coefficient h_{sf} defining heat transfer from the solid to the gas, and $z = 0$ is at the irradiated face of the absorber. The gas temperatures are defined by:

$$\dot{m}''\,c_p\,\frac{\partial T_{\mathrm{f}}}{\partial z} = h_{\mathrm{sf}}\,\bar{a}\,(T_{\mathrm{s}} - T_{\mathrm{f}}) \tag{4}$$

where $\dot{m}''$ is the mass flux of the gas over the absorber area. The equations are solved analytically by means of eigenvalues to determine the outlet temperature of the gas when given the temperatures of the gas and solid at the absorber front face, and a length of the absorber. The interfacial heat transfer coefficient is determined from experimental data in [25]. All calculations are done for an absorber with 20 ppi pore size. The system is always operated with a 50% weight sulphuric acid and 50% weight water mixture. When evaporated, sulfuric acid is decomposed into SO_3 and additional water. The resulting mixture is 86.6% H_2O and 13.4% SO_3 by molecular composition. Gas properties are taken for this mixture from the EES database or [26] at atmospheric pressure, and gas mixture properties are considered by molar weighted averages. An example of the solution of the solid and fluid temperatures is shown in Figure 5.

Equations (3-4) are coupled to a radiative heat transfer balance of the receiver considering the absorber front face, the window inner surface, and the cylindrical reactor wall. Standard view factors and the net radiation method are used to determine the temperature of the absorber front face [27].

$$E_{\mathrm{b}a} - \sum_{b=1}^{3} F_{a-b} E_{\mathrm{b}b} = \frac{\dot{q}_{\mathrm{rad},a}}{\epsilon_a} - \sum_{b=1}^{3}\left(\frac{1}{\epsilon_b} - 1\right) F_{a-b}\,\dot{q}_{\mathrm{rad},b} + H_{0a},\ a = 1,2,3 \tag{5}$$

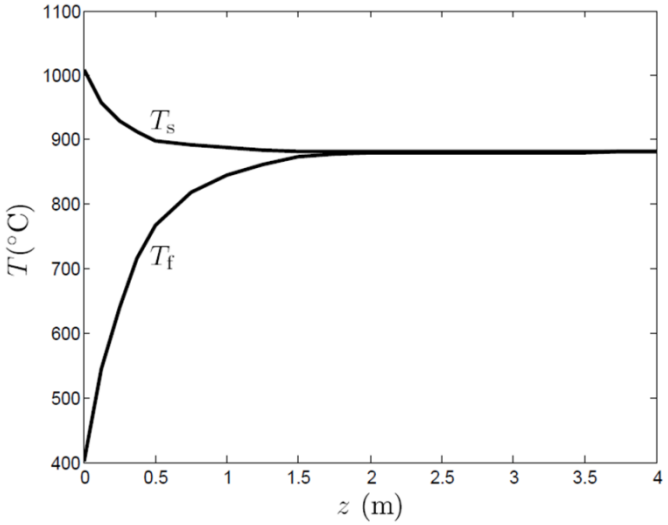

Figure 5: Solved fluid and solid temperatures along absorber axial direction for 1 l min^{-1} acid mixture.

Each of the three components is considered opaque and isothermal. The temperature of each surface is determined through the blackbody emittance E_b, while heat fluxes q''_{rad} are coupled to energy balances in each individual component. A factor, δ_{CSP} gives the fraction of solar energy transmitted through the window that is incident on the absorber, while the remainder is incident on the reactor walls.

$$A_{abs} H_{0,abs} = \delta_{CSP} q_{CSP,trans}, \quad A_{wall} H_{0,wall} = (1-\delta_{CSP}) q_{CSP,trans} \quad (6)$$

The window is modeled with a balance of heat fluxes:

$$q''_{CSP,abs} + (1-\tau_{in}) q''_{rad,window} = q''_{conv,outside} + q''_{emit,outside} \quad (7)$$

The absorbed flux from the concentrating system and the net flux from Eq. (5) are balanced against convective losses on the outside of the window, radiation emitted to the outside of the receiver, and radiation transmitted from the inside to outside of the receiver. Convection on the inside of the window is neglected based on expectations that the contribution to the total gas energy balance is small compared to the absorber, and to providing maximum possible estimates of window temperature. The convective term on the outside of the widow is modeled by a constant heat transfer coefficient h_{window} between the window temperature and ambient temperature. This factor will be tuned in experiments by forced ambient air flow over the window. The losses due to emission from the window are calculated by:

$$q''_{emi,outside} = \varepsilon_{window} \sigma \left(T^4_{window} - T^4_0 \right) \quad (8)$$

The transmittance of solar energy out of the reactor τ_{in}, is found from spectral data with respect to blackbody emission at effective temperatures of the absorber and receiver walls. The fractions of solar input transmitted, absorbed, and reflected are given by τ, ρ, and ε, averaged with respect to the solar spectrum from manufacturer data for fused quartz as used in [8,28]. These fractions are all portions of the total solar input, which is related to the solar flux on aperture by $I_{ap} A_{window} = q_{CSP}$. The aperture and window areas are considered equal.

The losses through the reactor insulation are coupled to the radiative transfer to the reactor wall through the wall inner temperature. Heat loss formulations for conduction through the insulation and for radiation and convection from the outer shell permit determination of the wall temperature.

$$q''_{rad,wall} A_{wall} = (T_{wall} - T_{shell}) A_{wall} \frac{k_{ins}}{\ln(r_{shell}/r_{wall})} = h_{shell} A_{shell} (T_{shell} - T_0) + \sigma \varepsilon_{shell} A_{shell} \left(T^4_{shell} - T^4_0 \right) \quad (9)$$

The equations were implemented in EES software and used for parametric analysis of the receiver performance, with a focus on component temperatures and in particular the outlet temperature of the fluid.

Results

For a basic set of input parameters, the solar flux on the aperture is varied to investigate temperatures of the system components, including the gas outlet temperature. The baseline parameter assumptions are given in . These baselines are used in later analysis unless otherwise specified.

Table 1: Baseline parameters for investigation of receiver performance.

Parameter	Symbol	Value
Absorber Diameter	D_{abs}	40 cm
Distance from Window to Absorber	L_{cav}	20 cm
Absorber Thickness	L_{abs}	4 cm
Insulation Thickness	L_{ins}	6 cm
Gas Inlet Temperature	$T_{f,0}$	400 °C
Sulfuric Acid Flow Rate	$\dot{V}_{SA,0}$	1 l min^{-1}
Aperture Radiative Flux	q''_{CSP}	450 kW m^{-2}
Fraction of Radiation on Absorber	δ_{CSP}	0.7
Absorber Emissivity	ε_{abs}	0.99
Insulation Thermal Conductivity	k_{ins}	0.31 W m^{-1} K^{-1}
Shell Emissivity	ε_{shell}	0.7
Window Heat Transfer Coefficient	h_{window}	50 W m^{-2} K^{-1}

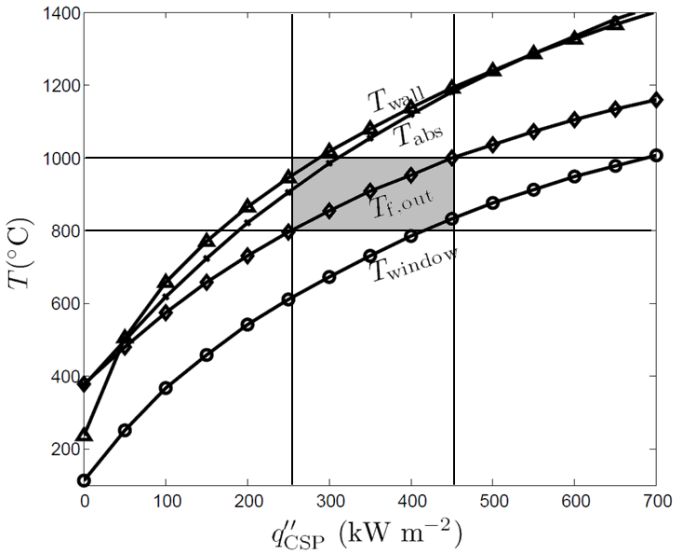

Figure 6: Effect of varying solar flux on system temperatures. Box given to show operating window based on fluid outlet temperatures.

shows the temperatures of system components with increasing heat flux on the aperture. The temperatures expectedly increase with increased solar flux, with non-linearity caused by radiative losses dependent on the fourth power of temperature. An operating window is defined on the plot due to the desire for fluid outlet temperatures between 800 and 1000 °C. This defines a desired solar flux range of 260 to 450 kW m^{-2}, which is specific to the geometry and flow rate for this case. Naturally, due to assuming radiation is all absorbed at the front surface, the absorber front temperature exceeds the fluid outlet temperature except for very low flux cases where the absorber cools the fluid. Therefore, these worse-case-scenario predicted absorber front temperatures are between 910 and 1190 °C, which are suitable for the Silicon Carbide material. Note that, with greater solar flux, there is a

larger deviation between absorber front temperature and fluid outlet temperature, as necessary for transfer of greater power density with a fixed surface area. The predicted window temperatures, between 610 and 830 °C, also fall within a suitable range for the quartz material of the window. These acceptable temperature ranges form a basis for design feasibility validated on the presented thermodynamic model.

An example of the parametric studies done to explore potential receiver designs is given in , where the diameter of the absorber (and window) is varied. The cavity is held cylindrical. With a larger absorber diameter, local solar flux decreases as the solar power on the aperture is held constant, reducing temperatures of all components. The increased area for heat transfer more effectively allows transfer of heat to the

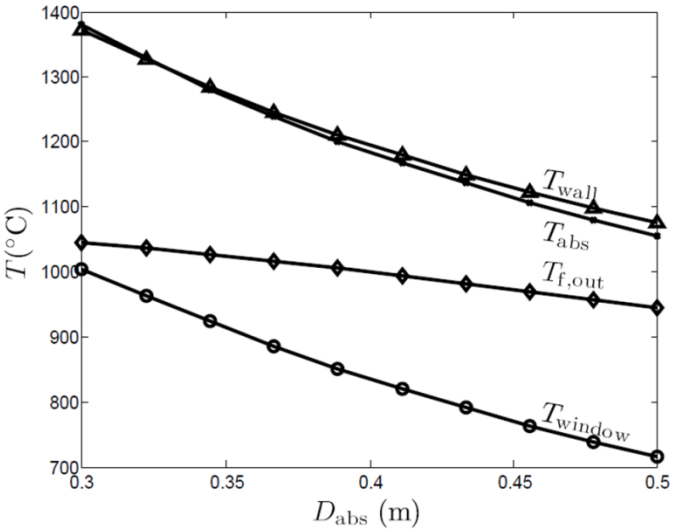

Figure 7: Parametric study of receiver diameter, resulting in varied component temperatures.

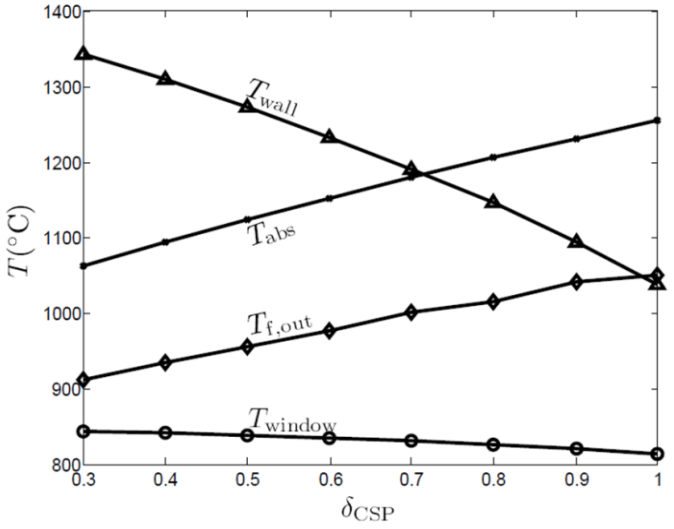

Figure 8: Variation in receiver component temperatures with varied values of δ_{CSP}, the fraction of incident radiation on the absorber.

gas outlet temperature decreases. However, the decrease of fluid outlet temperature with increased diameter but constant power and flow rate, indicates that greater thermal losses are present at higher diameters.

The results of this study were one aspect used to select a size for the absorber. Construction costs, design feasibility, and material safety factor were considered as well. Finally, the influence of the distribution of solar radiation from the heliostat field was also considered. An in-house ray tracing code was used to simulate the tower and heliostat field where the receiver will be tested, mapping the distribution of solar radiation on the absorber surface. Ray tracing results indicated that smaller diameters lead to a more uniform flux distribution. The balance of these factors led to the selection of a 40 cm absorber diameter for the receiver prototype. This case allows for gas outlet temperatures of 993 °C on a baseline set of conditions, meeting project goals. Similar parametric studies were completed to select other geometric parameters, such as insulation thickness and the distance between the window and absorber, given in , as well as considering geometries with unequal window and absorber radii. It was found that optimal results are found for a cylindrical receiver wall with the absorber placed at one absorber radius from the window.

To explore the effect of the solar field on thermal performance, without a complete coupling of solar field modeling and numerical heat transfer, the parameter δ_{CSP}, which gives the fraction of radiation entering the receiver which is incident on the absorber, is varied. The results of this parametric study are given in . With a larger fraction of radiation on the absorber, the absorber and fluid temperatures increase while wall temperatures decrease. Window temperatures are decreased with more radiation transferred to the absorber. Over a range of δ_{CSP} = [0.5,1], fluid outlet temperature varies less than 100 °C, indicating that a single receiver design is relatively flexible with respect to the distribution of incident radiation.

NUMERICAL HEAT TRANSFER AND FLUID FLOW MODELING

To investigate the distributions of temperatures, pressures, and fluid velocities within the volume of the receiver, a three-dimensional model accounting for heat and mass transfer was developed. As an exploration model, coupling of detailed radiative heat transfer was omitted in favor of parametric exploration based on possible scenarios for absorption of radiation throughout the silicon carbide volumetric absorber.

Methodology

Coupled mass, momentum, and energy conservation equations were solved at steady state. The following formulations give the porous media forms of the conservations equations, while simplification to fluid subdomains is resolved by simply setting ϕ to zero.

$$\nabla\cdot\left(\phi\rho\mathbf{v}\right)=0 \tag{10}$$

$$\nabla\cdot\left(\phi\rho\mathbf{v}\mathbf{v}\right)=-\phi\nabla p+\nabla\left(\phi\bar{\tau}\right)+\phi\mathbf{S}_{M} \tag{11}$$

Momentum conservation, in Equation 2, includes a source term for flow resistance through the porous media. This source term is formulated:

$$\mathbf{S}_M = -\left(\mathbf{D}\mathbf{v}_i + \mathbf{C}\frac{1}{2}\rho|\mathbf{v}|\mathbf{v} \right) \quad (12)$$

where the **D** and **C** matrices are diagonal matrices with elements of **D** given by viscosity divided by permeability *K*, and elements of **C** given by the inverse of the Dupuit-Forchheimer coefficient F_{DF}. Gravity effects are not considered.

Energy conservation is solved by separate equations for the gas and solid phases. An interfacial heat transfer term is included in both equations for heat exchanged between the phases. A source term accounting for radiative heat transfer is included only in the solid phase equation, under the assumption that the gas phase will be non-participating and radiative energy is first absorbed by the absorber before transferring to the gas. Chemical heat sources are not considered due to the relatively slow kinetics in the absence of catalysts compared to residence time [7].

$$\nabla \cdot \left(\phi \mathbf{v}_f \left(\rho_f E_f + p \right) \right) = \nabla \left(k_{eff,f} \nabla T_f + \phi \left(\bar{\tau}_{eff} \cdot \mathbf{v}_f \right) \right) + \bar{a} h_{sf} \left(T_f - T_s \right) \quad (13)$$

$$0 = \nabla \left(k_{eff,s} \nabla T_s \right) + \bar{a} h_{sf} \left(T_s - T_f \right) + q'''_{\text{src,rad}} \quad (14)$$

This set of governing equations is solved on a three dimensional mesh with a finite volume approach using ANSYS Fluent software. The domain consists of a bent inlet pipe, a gas volume between the absorber and window, the porous absorber, and a gas outlet region. The inlet is aligned radially from the receiver axis. In all regions other than the absorber, porosity is set to zero, reducing the governing equations to single phase. The mesh consists of 107,000 nodes, with dimensions shown in Figure 9.

A no-slip momentum boundary condition is used at all boundaries with the exception of the inlet and outlet. Except for the window, the energy equation boundary condition on these boundaries is a lumped heat transfer coefficient applied to account for heat transfer through the reactor body insulation. The heat transfer coefficient h_{lumped} is computed by:

$$\frac{1}{h_{\text{lumped}}} = \frac{1}{h_0} + \frac{\ln(r_{\text{out}} / r_{\text{in}}) r_{\text{out}}}{k_{\text{ins}}} \quad (15)$$

where h_0 is the outer surface convection coefficient, assumed to be 10 W m^{-2} K^{-1}. Heat losses are considered to be between the simulation boundary and an ambient heat sink at 300 K. The insulation is expected to be 10 cm thick, with conductivity k_{ins} of 0.35 W m^{-1} K^{-1}. For the geometry of Figure 9, h_{lumped} = 2.295 W m^{-2} K^{-1}. The window is set to a fixed temperature of 900 K, because, due to absorption of radiation in the window, a heat transfer coefficient condition is unreasonable, while cooling of the window by forced air flow will allow the temperature to be held fixed in practice.

The inlet is set to a normal direction, uniformly distributed specified mass flow of gas entering at 600 K, as would be heated by the electrical evaporator. The outlet is set to a fixed pressure of 1 atm.

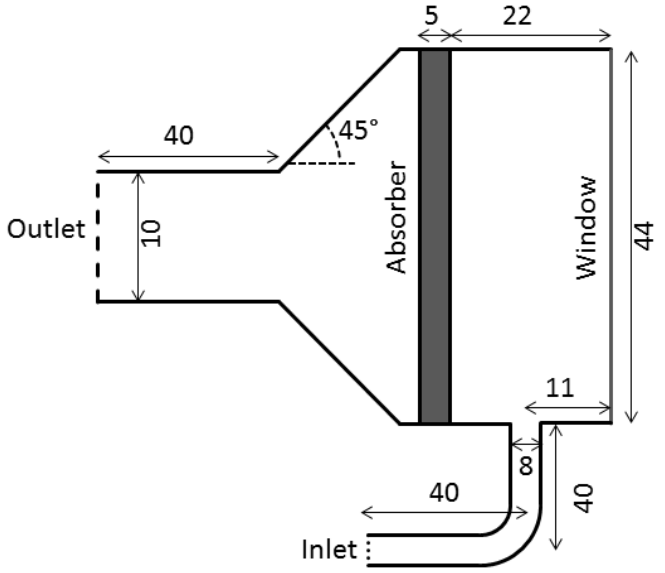

Figure 9: Analysis domain with key dimensions, given in cm. The inlet pipe enters the receiver in the radial direction.

The gas is an evaporated mixture of 50% weight sulfuric acid and 50% weight water. Basic properties for gaseous H_2O and SO_3 are taken from [26,29,30]. The mixture thermal conductivity is determined by the Wassiljewa equations [31], while viscosity is determined by the method of Wilke [32]. Effective specific heat is by a molar average. The gas is modeled as an ideal gas.

The absorber is considered porous pure SiC, with specific heat taken for SiC from [33], and density assumed constant at 3.21 g cm^{-3} [34]. The absorber is modeled with ϕ = 0.9, and assumed as a 20 ppi foam. Properties, flow resistance coefficients, and interfacial heat transfer coefficients are taken from results of pore level numerical simulations of a 20 ppi foam with similar porosity [35].

Based on the previously discussed isothermal fluid flow modeling of the receiver [24], a pressure drop layer is included directly on the downstream face of the absorber, to approximate an orifice plate that will be designed in the receiver to restrict flow. This layer was set with a pressure drop coefficient of $F_{DF}L$ of 3000 for all following results, which leads to about 30 pa of pressure drop for the default case of 1 l min^{-1} acid mixture flow rate.

Without a complete radiation model to couple heat generated in the absorber with input solar radiation, which is complex and computationally expensive, the effect of radiation distribution and power is explored parametrically using a heat source term in Eq. (14). A source term with a mathematical distribution of heat generation is introduced with varying shapes and total powers. First a uniform source term

distribution throughout the absorber is considered as an optimal baseline.

$$q'''_{src}(r,z) = q'''_0 \tag{16}$$

It is expected that radiation intensity will be greater at the center of the absorber than the edges, although radiative flux at the edges will not be near zero. It is also expected that the absorbed power will decrease through the thickness of the absorber. Therefore, two non-uniform distributions are considered, both with a linear decrease of absorbed power in the axial direction of radiation input. In the radial direction, and parabolic and linear distribution are the two shapes considered, both with peak values equal to 3.0 times the edge value of heat source.

$$q'''_{src}(r,z) = q'''_0 2\left[1+0.5\left(1-2\frac{r}{r_{max}}\right)\right]\left[1-\frac{z}{z_{max}}\right] \tag{17}$$

$$q'''_{src}(r,z) = q'''_0 2\left[1+0.5\left(1-2\left(\frac{r}{r_{max}}\right)^2\right)\right]\left[1-\frac{z}{z_{max}}\right] \tag{18}$$

The nominal heat generation rates q'''_0 must be calculated based on a total desired power by integrating the above equations over the volume of the absorber. For the default example, with a 5 cm thick, 44 cm diameter absorber with a total absorbed power of 30 kW, $q'''_0 = 3.948\times10^6$.

Results

Simulations of heat transfer to the fluid flowing through the porous absorber revealed key differences in behavior with variations in the distribution of solar absorption and with variations in fluid flow rate. Figure 10 shows the velocity distribution within the receiver for a default case of 1 l min^{-1} acid mixture and an absorbed power of 22.8 kW. This case uses the distribution of radiation source term in Eq. (18). Flow resistance by the absorber and pressure drop layer cause the flow to mix in the open zone between the absorber and window. Flow through the absorber is low velocity compared to the inlet flow, and mass flux is distributed relatively uniformly over the area of the absorber. For this case, the pressure drop layer provides an average of 30 pa of pressure drop, while the absorber provides an additional 20 pa. These results agree to within 10% with isothermal CFD simulations which determined that these small, millibar range pressure drops are sufficient to provide uniformity of the flow through the absorber, validating the usefulness of the isothermal simulations.

The flow field in the space between the absorber and the window shows a dispersive nature to the incoming flow stream near the inlet, with an impingement on the opposite wall, leading to recirculation cells forming along the window and absorber. Flow of the gas along the window is not detrimental, and may provide assistance in cooling the window. The primary dangers are if the window is over-cooled from the outer surface and acid condenses on the window, or if strong impingement at the window-shell interfaces could lead to failure of window sealing materials. Past the absorber, a laminar flow profile is developed as the gas exits the receiver. Colored vectors in

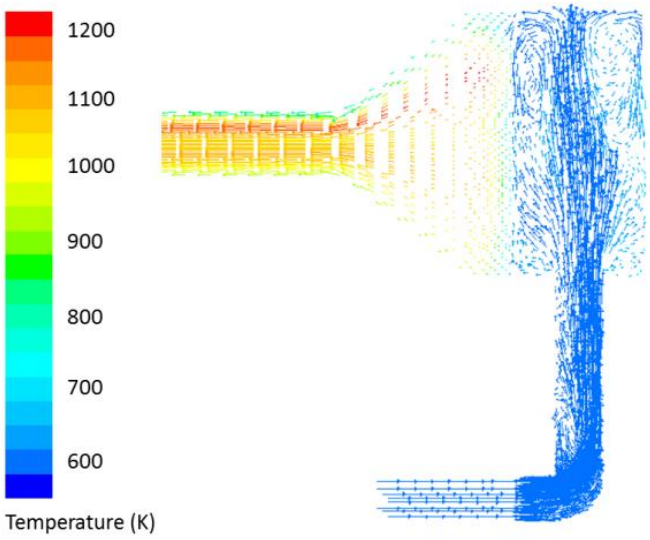

Figure 10: Velocity vectors, colored by temperature in K, showing flow through the receiver for the case of non-uniform solar absorption.

Figure 10 show the temperatures. The gas temperature non-uniformity at the exit of the absorber is still present in nearly the same form after the gas flows through the reducing cone and reaches the outlet. The distributions are similar but scaled to the diameters of absorber and outlet. This important finding must, in future work, be considered in analysis of the reactor that will be connected downstream, where the effects of a non-uniform temperature distribution at the reactor inlet may influence chemical conversion.

The effect of the heat source distribution within the absorber is important to determine the total heat transfer to the gas and the distribution in temperatures within the gas and absorber. Figure 11 shows the gas temperature distributions along the receiver midplane for the different heat source term cases. Identical total heat generation rates were applied to the absorber in all cases of 22.8 kW, but with different distributions. All cases have average gas outlet temperatures between 1237 K and 1257 K, so the distribution does not have a significant effect on the average gas temperature. Therefore, heat losses through the reactor body are not significantly affected by the distribution, which would be the primary cause of differences. However, changes in radiation losses due to localized high temperatures are not considered here. The uniform source term case naturally has the most uniform temperature distribution in the gas with maximum gas temperatures about 100 K greater than average gas outlet temperatures. It also shows the most visual non-symmetry due to the flow of gas from a single inlet, with variations up to 120 K between radial-opposite corresponding points. This vertical non-symmetry is similar in value for all cases, but only visible when radial variations from the heat source are minor.

The cases with non-uniform heat sources lead to variations in the gas temperature at the absorber exit of about 1000 K between the absorber center and edges. This temperature profile

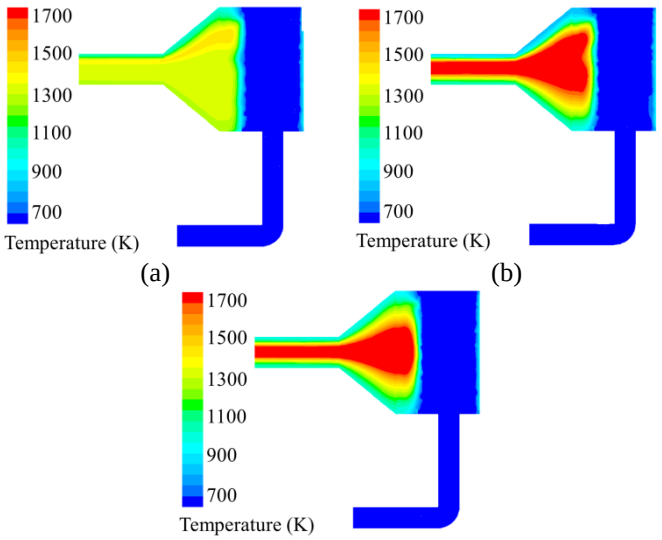

Figure 11: Fluid temperature contours in K, for cases of (a) uniform absorber heat source, (b) non-uniform parabolic heat source, and (c) non-uniform linear heat source.

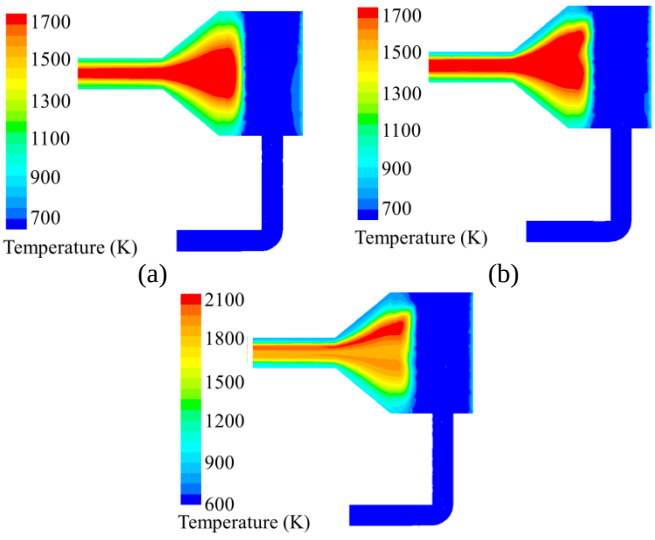

Figure 12: Fluid temperature contours in K, for varying gas flow rates, corresponding to (a) 0.5, (b) 1.0, and (c) 1.5 l min^{-1} liquid flow rate. Note that scales are not identical.

persists until the exit. In the case of the parabolic heat source term, a maximum absorber temperature was found to be 1816 K, a value that is above the normal operating limit of silicon carbide, but is also a likely overestimate due to re-radiation effects that are not directly considered.

In all cases, the highest absorber temperatures were found not on the surface facing the window, but at some location within the absorber, due to the gas flow cooling this surface. This result differs from results of the thermodynamic model which only considered radiation absorption by the absorber surface, but it must be confirmed with more detailed modeling including radiative heat transfer. Nevertheless, it is a desired characteristic of volumetric absorber systems to reduce re-radiation losses at the absorber face.

Variations in gas flow rate lead to important differences in system performance, so the inlet gas rate was varied between 0.6375 and 1.9125 kg min^{-1}, corresponding to 0.5 to 1.5 l min^{-1} of 50-50 weight mixture of water and sulfuric acid. The temperature distributions for varying gas flow rates are given in Figure 12. In order to achieve similar average outlet temperatures, the power generated by the source term must be set to 11, 23, and 34kW for the respective cases. An important determination is that a constant outlet temperature can be obtained in this system by increasing the input power proportionally to the gas flow rate. The implication is that there is not limitation on heat transfer area or rate between the absorber and the gas up to at least 1.5 l min^{-1} of acid mixture.

The cases of varying flow rates show differences in symmetry. For cases of low flow, the temperatures of gas and absorber show nearly perfect circumferential symmetry, despite only a single radial gas inlet. In higher flow cases, non-symmetry is clear, as greater inlet velocities lead to higher flow fractions following the opposite wall through the absorber, creating an area of low velocity inward from the high velocity zone. The high mass flux near the wall leads to lower temperatures, while the low velocity region reaches very high gas temperatures of over 2000 K. Though these temperatures are likely overestimates due to the inconsideration of detailed radiation transfer, the results indicate that high-power, high-flow rate cases are more likely to cause non-symmetrical temperature profiles with steeper gradients. These cases also necessitate higher radiative flux, at which uniformity in the radiative input is more difficult to achieve. Great care must be taken at high flow rate to ensure peak temperatures within the absorber are managed. Additional simulations confirmed that uniformity can be improved with larger pressure drops within the orifice plate, but at the expense of pressure differential on the window. Pressure drops through the receiver for the cases in Figure 12 are on average (a) 20, (b) 50, and (c) 100 pa.

Simulations were performed across a large number of heat generation powers and flow rates. The results are given in Figure 13. These curves show the increase in outlet temperature as power absorbed by the absorber increases. For each flow rate, a nearly linear curve is followed, with some curvature because the losses through the reactor body vary with temperature. To achieve an outlet temperature of 1000 °C, a total power on the absorber of 33 kW is necessary. This compares to 39.6 kW incident on the absorber from the thermodynamic model for the case of 450 kW m^{-2} solar flux. The agreement is good, considering the difference in assumptions of radiation absorption location. These results provide a performance guide used to achieve a desired outlet temperature.

General findings from the numerical heat transfer simulations provided benefits in determining locations for temperature measurements during operation of the prototype reactor. The non-uniformity in expected gas temperature has led

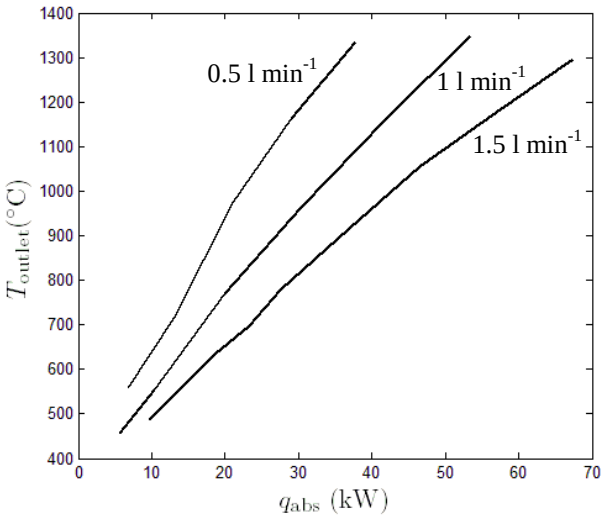

Figure 13: Average gas temperatures measured at the receiver outlet for varying liquid acid mixture flow rates and power absorbed by the silicon carbide absorber.

to a design with temperature measurements of the gas flow as it exits the absorber and within the conical reducer section of the receiver. Future work to validate the simulation and to understand operation has been aided greatly by initial results to determine expected behavior and measurement locations.

CONCLUSIONS AND FUTURE OUTLOOK

The work presented is an overview of approaches that are used to drive the design and operation of a test receiver for superheating evaporated sulfuric acid for chemical cycling. The benefit of the multi-approach methodology is that design questions are answered by the most appropriate and resource effective model. Individual models have been applied to focus on three-dimensional fluid flow, on reactor geometry and operating window, and on thermal distributions. The results from simulations have led to a design for a prototype receiver that will be part of a 100 kW pilot plant for experimental on-sun operation.

Key aspects of the design that were found by simulation results were the single, radial gas inlet, a cylindrical, 40 cm diameter receiver geometry, and an operating window of absorber temperatures and gas flow rates that will drive the experimental campaign. Numerical simulations indicate that a non-uniform distribution of absorbed radiation in the absorber lead to large variations in the gas temperatures at outlet, and potentially more importantly, large variations in temperature of the silicon carbide absorber, which may lead to significant mechanical problems. These results have furthered the design efforts of the receiver to consider detailed studies of the solar field to achieve maximum uniformity of the solar input on the absorber, as well as future improvements to the model to accurately model the radiation inside the receiver.

In the future, the numerical heat transfer model of the receiver will be expanded to model radiative heat transfer as well as window and insulation components. Radiation modeling is expected to account for transfer between surfaces and within the participating absorber. Ray-tracing simulations of the experimental solar field will be used to provide realistic radiative boundary conditions. Thermodynamic analysis will be coupled to models of the adiabatic reactor to explore the influence of gas outlet temperatures from the receiver and better define experimental goals. Finally, results from both models will be compared to experimental results from on-sun tests.

ACKNOWLEDGMENTS

This work has been funded under the Fuel Cell Hydrogen – Joint Undertaking (FCH-JU) project Sol2Hy2, contract no. 325320. The authors would like to acknowledge model development efforts by Jan Drescher, design collaboration with Dr. Moises Romero, and modeling consultations with Prof. Sophia Haussener.

REFERENCES

[1] Brecher, L. E., Spewock, S., and Warde, C. J., 1977, "The Westinghouse Sulfur Cycle for the Thermochemical Decomposition of Water." International Journal of Hydrogen Energy, 2, pp. 7–15.

[2] Kolb, G. J., and Diver, R. B., 2008, "Screening Analysis of Solar Thermochemical Hydrogen Concepts." Sandia National Laboratories, Albuquerque.

[3] Broggi, A., Langenkamp, H., Mertel, G., and van Velzen, D., 1982, "Decomposition of Sulfuric Acid by the Cristina Process-A Status Report." Hydrogen Energy Progress, 2, pp. 611-621.

[4] Kolb, G., Diver, R. B., and Siegel, N., 2007. "Central-station Solar Hydrogen Power Plant." Journal of Solar Energy Engineering, 129, pp. 179–183.

[5] General Atomics, 1985, "Decomposition of Sulfuric Acid Using Solar Thermal Energy." GA-A17573.

[6] General Atomics, 1986, "High-Pressure Catalytic Metal Reactor in a Simulated Solar Central Receiver." GA-A18285.

[7] Roeb, M., Monnerie, N., Houaijia, A., Thomey, D., Sattler, C., 2013, "Solar Thermal Water Splitting." *Renewable Hydrogen Technologies*. Gandía, L. M., Arzamendi, G., Diéguez, P. M., eds., Elsevier, Amsterdam, pp. 63–86.

[8] Thomey, D., de Oliveira, L., Säck, J. P., Roeb, M., and Sattler, C., 2012, "Development and Test of a Solar Reactor for Decomposition of Sulphuric Acid in Thermochemical Hydrogen Production." International Journal of Hydrogen Energy, 37, pp. 16615–16622.

[9] Ávila-Marín, A. L., 2011 "Volumetric Receivers in Solar Thermal Power Plants with Central Receiver System Technology: A Review." Solar Energy, 85, pp. 891–910.

[10] Veeraragavan, A., Lenert, A., Yilbas, B., Al-Dini, S., and Wang, E. N., 2012, "Analytical Model for the Design of Volumetric Solar Flow Receivers." International Journal of Heat and Mass Transfer, 31, pp. 556–564.

[11] Ahlbrink, N., Belhomme, B., and Pitz-Paal, R., 2009, "Modeling and Simulation of a Solar Tower Power Plant with Open Volumetric Air Receiver." Proceedings of the 7th Modelica Conference, Como, Italy.
[12] Skocypec, R. D., Boehm, R. F., and Chavez, J. M., 1988, "Heat Transfer Modeling of the IEA/SSPS Volumetric Receiver." Journal of Solar Energy Engineering, 111, pp. 138–143.
[13] Muir, J. F., Hogan, R. E., Skocypec, R. D., and Buck, R., 1993, "The CAESAR Project: Experimental and Modeling Investigations of Methane Reforming in a Catalytically Enhanced Solar Absorption Receiver on a Parabolic Dish, NASA STI/Recon Technical Report No. 94, 19109.
[14] Wu, Z., Caliot, C., Flamant, G., and Wang, Z., 2011, "Coupled Radiation and Flow Modeling in Ceramic Foam Volumetric Solar Air Receivers." Solar Energy, 85, pp. 2374–2385.
[15] Villafán-Vidales, H. I., Abanades, S., Caliot, C., and Romero-Paredes, H., 2011, "Heat Transfer Simulation in a Thermochemical Solar Reactor Based on a Volumetric Porous Receiver." Applied Thermal Engineering, 31, pp. 3377–3386.
[16] Hischier, I., Hess, D., Lipiński, W., Modest, M., and Steinfeld, A., 2010, "Heat Transfer Analysis of a Novel Pressurized Air Receiver for Concentrated Solar Power via Combined Cycles." Journal of Thermal Science and Engineering Applications, 1, 041002.
[17] He, Y. L., Cheng, Z. D., Cui, F. Q., Li, Y., and Li, D., 2012, "Numerical Investigations on a Pressurized Volumetric Receiver: Solar Concentrating and Collecting Modeling." Renewable Energy, 44, pp. 368–379.
[18] Crocker, A., and Miller, F., 2011, "Coupled Fluid Flow and Radiative Modeling for a Small Particle Solar Receiver." 9th Annual International Energy Conversion Engineering Conference, San Diego, California.
[19] Becker, M., Fend, Th., Hoffschmidt, B., Pitz-Paal, R., Reutter, O., Stamatov, V., Steven, M., and Trimis, D., 2005, "Theoretical and Numerical Investigation of Flow Stability in Porous Materials Applied as Volumetric Solar Receivers." Solar Energy, 80, pp. 1241–1248.
[20] Roeb, M., Thomey, D., Graf, D., Sattler, C., Poitou, S., Pra, F., et al., 2011, "HycycleS: a Project on Nuclear and Solar Hydrogen Production by Sulphur-Based Thermochemical Cycles." International Journal of Nuclear Hydrogen Production and Applications, 2, pp. 202–226.
[21] Noglik, A., Roeb, M., Sattler, C., and Pitz-Paal, R., 2011, "Modeling of a Solar Receiver-Reactor for Sulfur-Based Thermochemical Cycles for Hydrogen Generation." International Journal of Energy Research, 35, pp. 449–458.
[22] Haussener, S., Thomey, D., Roeb, M., and Steinfeld, A., 2012, "Multi-Scale Modeling of a Solar Reactor for the High-Temperature Step of a Sulphur-Iodine-Based Water Splitting Cycle." Proceedings of the ASME 2012 Heat Transfer Summer Conference, Rio Grande, Puerto Rico.
[23] Noglik, A., Roeb, M., Sattler, C., and Pitz-Paal, R., 2011, "Numerical Analysis of Operation Conditions and Design Aspects of a Sulfur Trioxide Decomposer for Solar Energy Conversion." International Journal of Energy Research, 36, pp. 798–808.
[24] Schwan, S. P., 2014, "Strömungssimulation Solarreceiver. Optimierung der Einströmung in den Solarreceiver des Sol2Hy2-Projekts." Project Report, Cologne University of Applied Sciences, Cologne, Germany.
[25] Becker, M., Fend, T., Hoffschmidt, B., and Reutter, O., 2002, "Thermisch Beaufschlagte Porenkörper und deren Durchströmungs- und Wärmeübertragungseigenschaften: DFG Projekt DU 101/55-1", Deutsches Zentrum für Luft- und Raumfahrt.
[26] Chase, M.W., 1998, "NIST-JANAF Thermochemical Tables." Journal of Physical and Chemical Reference Data. Monograph, 9.
[27] Modest, M,F., 2003, *Radiative Heat Transfer*, 2nd Ed., Academic Press, San Diego.
[28] Heraeus, "Standart optics Information: HOQ 310", http://optics.heraeus-quarzglas.com/media/webmedia_local/datenbltter/O434M_HOQ.pdf, accessed 12 May 2014
[29] Liessmann, G., Schmidt, W., and Reiffarth, S., 1995, *Data Compilation of the SaechsischeOlefinwerke Boehln, Germany.*
[30] Reid, R. C., Prausnitz, J. M., and Sherwood, T. K., 1987, *The Properties of Gases and Liquids, 4th Ed*, McGraw-Hill, New York.
[31] Wassiljewa, A., 1904, Physik Z, 5, 737.
[32] Wilke, C. R., 1950, "A Viscosity Equation for Gas Mixtures." Journal of Chemical Physics, 18, pp. 517-519.
[33] Jang, B.-K., and Sakka, Y., 2007, "Thermophysical Properties of Porous SiC Ceramics Fabricated by Pressureless Sintering." Science and Technology of Advanced Materials, 8, pp. 655–659.
[34] Patnaik, P., 2002, *Handbook of Inorganic Chemicals*, McGraw-Hill, New York.
[35] Haussener, S., 2010, "Tomography-Based Determination of Effective Heat and Mass Transport Properties of Complex Multi-phase Media." Ph. D. thesis, ETH Zurich, Zurich, Switzerland.